

Datasheet for 610-145-002-0.5

Mouse IgG (H&L) Antibody DyLight™ 800 Conjugated

Overview

Description:	Goat Anti-Mouse IgG (H&L) Antibody DyLight™ 800 Conjugated (5 X 100 µg) - 610-145-002-0.5
Item No.:	610-145-002-0.5
Size:	5 x 100 µg
Applications:	Dot Blot, WB, IF, IHC
Reactivity:	Mouse
Host Species:	Goat

Product Details

Background:	Anti-Mouse IgG DyLight 800 Antibody generated in goat detects reactivity to Mouse IgG. Secreted as part of the adaptive immune response by plasma B cells, immunoglobulin G constitutes 75% of serum immunoglobulins. Immunoglobulin G binds to viruses, bacteria, as well as fungi and facilitates their destruction or neutralization via agglutination (and thereby immobilizing them), activation of the compliment cascade, and opsonization for phagocytosis. The whole IgG molecule possesses both the F(c) region, recognized by high-affinity Fc receptor proteins, as well as the F(ab) region possessing the epitope-recognition site. Both the Heavy and Light chains of the antibody molecule are present. Secondary Antibodies are available in a variety of formats and conjugate types. When choosing a secondary antibody product, consideration must be given to species and immunoglobulin specificity, conjugate type, fragment and chain specificity, level of cross-reactivity, and host-species source and fragment composition.
Synonyms:	Goat Anti-Mouse IgG Secondary Antibody DyLight™800 Conjugated, Goat Anti-Mouse IgG Antibody DyLight™800 Conjugated, Anti-mouse IgG secondary antibody, anti-mouse IgG DyLight™800 conjugated secondary antibody
Host Species:	Goat
Specificity:	IgG (H&L)
Conjugate:	DyLight™ 800
Clonality:	Polyclonal
Format:	IgG
F/P Ratio:	2.7

Specific Activity: 1.6

Target Details

Reactivity: Mouse

Immunogen: Mouse IgG, whole molecule

Purity/Specificity: This product was prepared from monospecific antiserum by immunoaffinity chromatography using Mouse IgG coupled to agarose followed by conjugation to fluorochrome and extensive dialysis against the buffer stated above. Assay by immunoelectrophoresis resulted in a single precipitin arc against anti-Goat Serum, Mouse IgG and Mouse Serum. This antibody will react with heavy chains of Mouse IgG and with light chains of most Mouse immunoglobulins.

Application Details

Tested Applications: Dot Blot, WB

Suggested Applications: IF, IHC (Based on references)

Application Note: Anti-Mouse IgG DyLight 800 Antibody has been tested by dot blot and western blot and is designed for immunofluorescence microscopy, fluorescence based plate assays (FLISA) and fluorescent western blotting. This product is also suitable for multiplex analysis, including multicolor imaging, utilizing various commercial platforms. The emission spectra for this DyLight™ conjugate match the principle output wavelengths of most common fluorescence instrumentation.

Assay Dilutions: All assays should be optimized by the user. Recommended dilutions (if any) may be listed below.

FLISA: >1:20,000

IF: >1:5,000

WB: >1:10,000

Formulation

Physical State: Lyophilized

Concentration: 1.0 mg/mL by UV absorbance at 280 nm

Buffer: 0.02 M Potassium Phosphate, 0.15 M Sodium Chloride, pH 7.2

Preservative: 0.01% (w/v) Sodium Azide

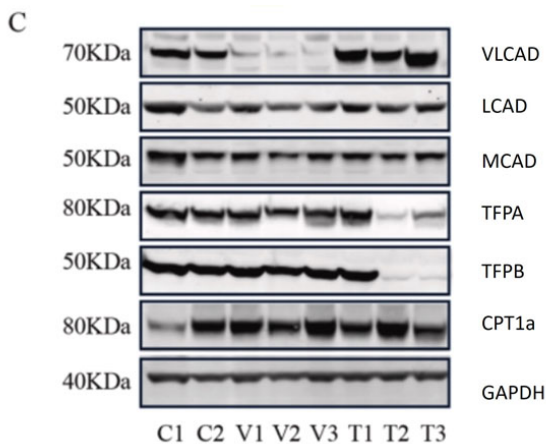
Stabilizer: 10 mg/mL Bovine Serum Albumin (BSA) - Immunoglobulin and Protease free

Reconstitution Volume:	100 μ L
Reconstitution Buffer:	Restore with deionized water (or equivalent)

Shipping & Handling

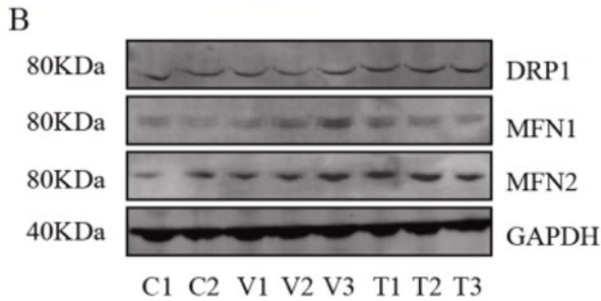
Shipping Condition:	Ambient
Storage Condition:	Store vial at 4° C prior to restoration. For extended storage aliquot contents and freeze at -20° C or below. Avoid cycles of freezing and thawing. Centrifuge product if not completely clear after standing at room temperature. This product is stable for several weeks at 4° C as an undiluted liquid. Dilute only prior to immediate use.
Expiration:	Expiration date is one (1) year from date of receipt.

Images



Western Blot

C. Representative western blots, original blots are shown in (supplementary Fig S8-9). And densitometric quantification of relative protein levels from western blots. Data are depicted as mean \pm SD, n = 3, **P < 0.01, ***P < 0.001 and ****P < 0.0001 by one-way ANOVA. Intracellular transport, activation, mitochondrial transport, β -oxidation, carnitine shuttle, and auxiliary proteins. The primary antibodies used as follows: VLCAD 1:1000, MCAD 1:1000, LCAD 1:1000, TFPA 1:500, TFPb 1:3000, CPT1 α 1:1000, and GAPDH 1:30,000 dilutions overnight at 4 °C. The membranes were then incubated with fluorescent conjugated secondary antibodies for 1 h; DyLight 800 conjugated goat Anti-Rabbit IgG (611-145-002), DyLight 680 conjugated goat Anti-Rabbit IgG (611-144-003), DyLight 800 conjugated goat Anti-Mouse IgG (610-145-002), and DyLight 680 conjugated donkey Anti-Mouse IgG (610-744-124). Fig 1. PMID: 33725513.

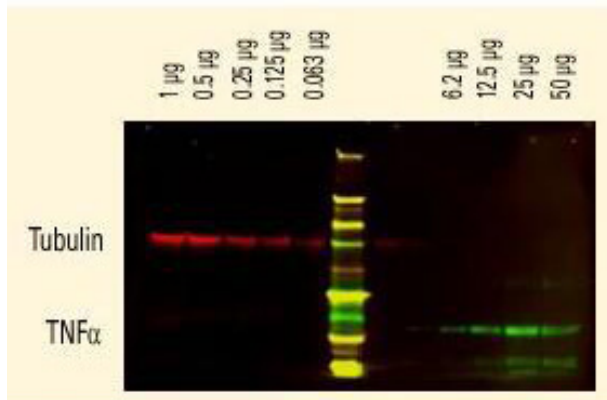








Western Blot

Assessment of mitochondrial fusion and fission. B. Representative western blots (original blots are shown in supplementary Fig. S10) and quantification of MFN1/2 and DRP1. No significant changes in the relative levels of proteins that facilitate mitochondrial fusion (MFN1/2) and fission (DRP1) between non-disease (control) and mutant primary fibroblasts. Data are depicted as mean \pm SD, n = 3. The primary antibodies used as follows: MFN1 1:400, MFN2 (1:400, DRP1 1:100 and GAPDH 1:30,000 dilutions overnight at 4 °C. The membranes were then incubated with fluorescent conjugated secondary antibodies for 1 h; DyLight 800 conjugated goat Anti-Rabbit IgG (611-145-002), Antibody DyLight 680 conjugated Anti-Rabbit IgG made in goat (611-144-003), DyLight 800 conjugated goat Anti-Mouse IgG (610-145-002), and DyLight 680 conjugated donkey Anti-Mouse IgG (610-744-124). Fig 3. PMID: 33725513.

Western Blot

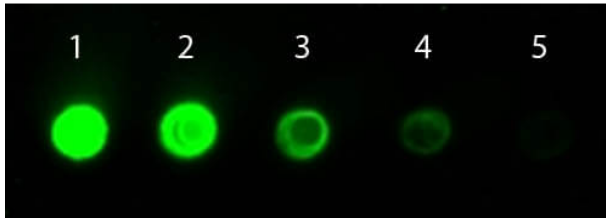
DyLight™ dyes can be used for two-color Western Blot detection with low background and high signal. Anti-tubulin was detected using a DyLight™ 680 conjugate. Anti-TNF α was detected using a DyLight™ 800 conjugate. The image was captured using the Odyssey® Infrared Imaging System developed by LI-COR.



Emission	Color	DyLight™ Dye	Ex/Em (nm)	ϵ ($M^{-1} cm^{-1}$)	Similar Dyes
Blue		405	400/420	30,000	Alexa™ 405, Cascade Blue
Green		488	493/518	70,000	Alexa™ 488, Cy2®, FITC
Yellow		549	550/568	150,000	Alexa™ 546, Alexa 555, Cy3®, TRITC
Red		649	646/674	250,000	Alexa™ 647, Cy5®
Near Infrared		680	682/715	140,000	Alexa™ 680, Cy5.5®, IRDye™ 700
Infrared		800	770/794	270,000	IRDye™ 800

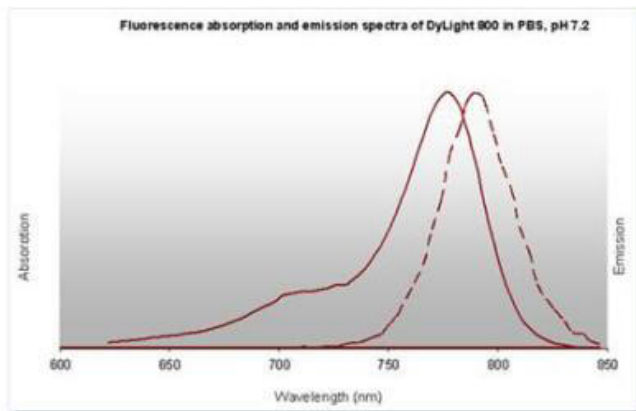
Diagram

Properties of DyLight™ Fluorescent Dyes.



Dot Blot

Dot Blot of Goat anti-Mouse IgG Antibody DyLight 800 Conjugated. Antigen: Mouse IgG. Load: Lane 1 - 100 ng Lane 2 - 33.3 ng Lane 3 - 11.1 ng Lane 4 - 3.70 ng Lane 5 - 1.23 ng. Primary antibody: none. Secondary antibody: Goat anti-Mouse IgG Antibody DyLight 800 Conjugated at 1:1,000 for 60 min at RT. Block: MB-070 for 60 min at RT.



Diagram

DyLight™ 800 Fluorescence Spectra

References

- Meric-Bernstam F et al. Antitumor Activity and Biomarker Analysis for TROP2 Antibody-Drug Conjugate Datopotamab Deruxtecan in Patient-Derived Breast Cancer Xenograft Models. *Clin Cancer Res.* (2025)
- Baumann V et al. Faa1 membrane binding drives positive feedback in autophagosome biogenesis via fatty acid activation. *J Cell Biol.* (2024)
- Li L et al. Microglia Autophagy Mediated by TMEM166 Promotes Ischemic Stroke Secondary to Carotid Artery Stenosis. *Aging Dis.* (2024)
- Voß Y et al. Malaria parasite centrins can assemble by Ca²⁺-inducible condensation. *PLoS P et al.* (2023)
- Wu W et al. SARS-CoV-2 N protein induced acute kidney injury in diabetic db/db mice is associated with a Mincle-dependent M1 macrophage activation. *Front Immunol.* (2023)
- Zhang L et al. Interleukin 6 (IL-6) Regulates GABAA Receptors in the Dorsomedial Hypothalamus Nucleus (DMH) through Activation of the JAK/STAT Pathway to Affect Heart Rate Variability in Stressed Rats. *Int J Mol Sci.* (2023)

- Arroum T et al. Loss of respiratory complex I subunit NDUFB10 affects complex I assembly and supercomplex formation. *Biol Chem.* (2023)
- Lopez J et al. The ribosomal S6 kinase 2 (RSK2)-SPRED2 complex regulates the phosphorylation of RSK substrates and MAPK signaling. *J Biol Chem.* (2023)
- Dabrowski R et al. Parallel phospholipid transfer by Vps13 and Atg2 determines autophagosome biogenesis dynamics. *J Cell Biol.* (2023)
- Cuevas-Navarro A et al. RAS-dependent RAF-MAPK hyperactivation by pathogenic RIT1 is a therapeutic target in Noonan syndrome-associated cardiac hypertrophy. *Sci Adv.* (2023)
- Jung HE et al. Intranasal delivery of an adenovirus-vector vaccine co-expressing a modified spike protein and a genetic adjuvant confers lasting mucosal immunity against SARS-CoV-2. *Antiviral Res.* (2023)
- Nitschke L et al. Alternative splicing mediates the compensatory upregulation of MBNL2 upon MBNL1 loss-of-function. *Nucleic Acids Res.* (2023)
- Winter JM et al. Collateral deletion of the mitochondrial AAA+ ATPase ATAD1 sensitizes cancer cells to proteasome dysfunction. *Elife.* (2022)
- Doerfler AM et al. LPA disruption with AAV-CRISPR potently lowers plasma apo(a) in transgenic mouse model: A proof-of-concept study. *Mol Ther Methods Clin Dev.* (2022)
- Tao, X et al. Phenylbutyrate modulates polyamine acetylase and ameliorates Snyder-Robinson syndrome in a Drosophila model and patient cells. *Jci Insight* (2022)
- Wang, Q et al. STING agonism reprograms tumor-associated macrophages and overcomes resistance to PARP inhibition in BRCA1-deficient models of breast cancer. *Nature Communications* (2022)
- Orengo, JP et al. Reduction of mutant ATXN1 rescues premature death in a conditional SCA1 mouse model. *JCI Insight* (2022)
- Wang B et al. Intracerebral hemorrhage alters $\alpha\delta 1$ and thrombospondin expression in rats. *Exp Ther Med.* (2022)
- De Giorgi M et al. Targeting the ApoA1 locus for liver-directed gene therapy. *Mol Ther Methods Clin Dev.* (2021)
- Cuevas-Navarro A et al. The RAS GTPase RIT1 compromises mitotic fidelity through spindle assembly checkpoint suppression. *Curr Biol.* (2021)
- Watt AC et al. CDK4/6 inhibition reprograms the breast cancer enhancer landscape by stimulating AP-1 transcriptional activity. *Nat Cancer.* (2021)
- Zhang B et al. Dominant Role of PI3K p110 α over p110 β in Insulin and β -Adrenergic Receptor Signalling. *Int J Mol Sci.* (2021)
- Nuebel E et al. The biochemical basis of mitochondrial dysfunction in Zellweger Spectrum Disorder. *EMBO Rep.* (2021)
- Raimo S et al. Mitochondrial morphology, bioenergetics and proteomic responses in fatty acid oxidation disorders. *Redox Biol.* (2021)
- Nitschke L et al. Modulation of ATXN1 S776 phosphorylation reveals the importance of allele-specific targeting in SCA1. *JCS Insight.* (2021)
- Schutter M et al. Local fatty acid channeling into phospholipid synthesis drives phagophore expansion during autophagy. *Cell.* (2020)

- Bensard CL et al. Regulation of tumor initiation by the mitochondrial pyruvate carrier. *Cell Metab.* (2020)
- Zhan T et al. Cangrelor alleviates bleomycin-induced pulmonary fibrosis by inhibiting platelet activation in mice. *Mol Immunol.* (2020)
- Bacman SR et al. Manipulation of mitochondrial genes and mtDNA heteroplasmy. *Methods Cell Biol.* (2020)
- Ma X et al. Nicotinamide mononucleotide adenyltransferase uses its NAD⁺ substrate-binding site to chaperone phosphorylated Tau. *Elife.* (2020)
- Navarro R et al. TGF- β -induced IGFBP-3 is a key paracrine factor from activated pericytes that promotes colorectal cancer cell migration and invasion. *Mol Oncol.* (2020)
- Kennedy T et al. Genetic background mutations drive neural circuit hyperconnectivity in a fragile X syndrome model. *BMC Biol.* (2020)
- Asthana V et al. Development of a Novel Class of Self-Assembling dsRNA Cancer Therapeutics: a Proof of Concept Investigation. *Mol Ther Oncolytics.* (2020)
- Mitra S, Bodor DL, David AF, et al. Genetic screening identifies a SUMO protease dynamically maintaining centromeric chromatin. *Nat Commun.* (2020)
- Nowinski SM et al. Mitochondrial fatty acid synthesis coordinates oxidative metabolism in mammalian mitochondria. *Elife* (2020)
- Li R et al. RNF115 deletion inhibits autophagosome maturation and growth of gastric cancer *Cell Death Dis.* (2020)
- Woods BL. et al. Interplay of septin amphipathic helices in sensing membrane-curvature and filament bundling. *bioRxiv* (2020)
- Araiz et al. Enhanced β -adrenergic signalling underlies an age-dependent beneficial metabolic effect of PI3K p110 α inactivation in adipose tissue. *Nature Communications* (2019)
- Hong D et al. Deletion of TMEM268 inhibits growth of gastric cancer cells by downregulating the ITGB4 signaling pathway. *Cell Death Differ.* (2019)
- Yu S et al. RSRC1 suppresses gastric cancer cell proliferation and migration by regulating PTEN expression. *Mol Med Rep.* (2019)
- Wang M et al. Native Polyacrylamide Gel Electrophoresis Immunoblot Analysis of Endogenous IRF5 Dimerization. *J Vis Exp.* (2019)
- Bailetti AA et al. Enhancer of Polycomb and the Tip60 complex repress hematological tumor initiation by negatively regulating JAK/STAT pathway activity. *Dis Model Mech.* (2019)
- Subramanian J et al. CPG15/neuritin mimics experience in selecting excitatory synapses for stabilization by facilitating PSD95 recruitment. *Cell Rep.* (2019)
- Latorre-Pellicer A et al. Regulation of mother-to-offspring transmission of mtDNA heteroplasmy. *Cell Metab.* (2019)
- Campbell LA et al. Gesicle-mediated delivery of CRISPR/Cas9 ribonucleoprotein complex for inactivating the HIV provirus. *Mol Ther.* (2019)
- Jarrett KE et al. Somatic Editing of Ldlr With Adeno-Associated Viral-CRISPR Is an Efficient Tool for Atherosclerosis Research. *Arterioscler Thromb Vasc Biol.* (2018)

- Zhan TW et al. Cangrelor alleviates pulmonary fibrosis by inhibiting GPR17-mediated inflammation in mice. *Int Immunopharmacol.* (2018)
- Bacman SR et al. MitoTALEN reduces mutant mtDNA load and restores tRNA Ala levels in a mouse model of heteroplasmic mtDNA mutation. *Nat Med.* (2018)
- Haapalainen et al. Expression of CPPED1 in human trophoblasts is associated with timing of term birth. *Journal of Cellular and Molecular Medicine* (2018)
- Lin et al. Liver-specific deletion of Eva1a/Tmem166 aggravates acute liver injury by impairing autophagy. *Cell Death & Disease* (2018)
- Zhang et al. Amelioratory Effects of Testosterone Propionate on Age-related Renal Fibrosis via Suppression of TGF- β 1/Smad Signaling and Activation of Nrf2-ARE Signaling. *Scientific Reports* (2018)
- Bacman, SR et al. MitoTALEN reduces mutant mtDNA load and restores tRNAAla levels in a mouse model of heteroplasmic mtDNA mutation. *Nature Medicine* (2018)
- Yu S et al. PPP2R2D, a regulatory subunit of protein phosphatase 2A, promotes gastric cancer growth and metastasis via mechanistic target of rapamycin activation. *Int J Oncol.* (2018)
- Jarrett et al. Somatic genome editing with CRISPR/Cas9 generates and corrects a metabolic disease. *Scientific Reports* (2017)
- Li et al. Deletion of Pgcd5 in mice led to the deficiency of placenta development and embryonic lethality. *Cell Death & Disease* (2017)
- Xia et al. Knockout of MARCH2 inhibits the growth of HCT116 colon cancer cells by inducing endoplasmic reticulum stress. *Cell Death & Disease* (2017)
- Shen et al. EMC6/TMEM93 suppresses glioblastoma proliferation by modulating autophagy. *Cell Death & Disease* (2016)
- Xia D et al. MARCH2 regulates autophagy by promoting CFTR ubiquitination and degradation and PIK3CA-AKT-MTOR signaling. *Autophagy.* (2016)
- Wang Z et al. PHF23 (plant homeodomain finger protein 23) negatively regulates cell autophagy by promoting ubiquitination and degradation of E3 ligase LRSAM1. *Autophagy.* (2014)
- Li Y et al. A novel ER-localized transmembrane protein, EMC6, interacts with RAB5A and regulates cell autophagy. *Autophagy.* (2013)
- Viorela Pop et al. Early brain injury alters the blood-brain barrier phenotype in parallel with β -amyloid and cognitive changes in adulthood. *J Cereb Blood Flow Metab.* (2013)

Disclaimer

This product is for research use only and is not intended for therapeutic or diagnostic applications. Please contact a technical service representative for more information. All products of animal origin manufactured by Rockland Immunochemicals are derived from starting materials of North American origin. Collection was performed in United States Department of Agriculture (USDA) inspected facilities and all materials have been inspected and certified to be free of disease and suitable for exportation. All properties listed are typical characteristics and are not specifications. All suggestions and data are offered in good faith but without guarantee as conditions and methods of use of our products are beyond our control. All claims must be made within 30 days following the date of delivery. The prospective user must determine the suitability of our materials before adopting them on a commercial scale. Suggested uses of our products are not recommendations to use our products in violation of any patent or as a license under any patent of Rockland Immunochemicals, Inc. If you require a commercial license to use this material and do not have one, then return this material, unopened to: Rockland Inc., P.O. BOX 5199, Limerick, Pennsylvania, USA.